Dalton Transactions

ROYAL SOCIETY OF CHEMISTRY

PAPER

View Article Online
View Journal

Cite this: DOI: 10.1039/d2dt01154a

Aggregation of gold(I) complexes: phosphorescence *vs.* singlet oxygen production†

Andrea Pinto, *[a,b] Jas S. Ward, [c] Kari Rissanen, [c] Martin Smith [d] and Laura Rodríguez *[a,b]

Received 13th April 2022,
Accepted 13th May 2022

DOI: 10.1039/d2dt01154a

rsc.li/dalton

Herein we report on the synthesis of six new phosphane-gold(I)-4-ethynylaniline complexes (neutral and cationic), with a tris-naphthalene substituted tertiary phosphane bearing a secondary amine as a linker and containing different halogen groups (Cl and Br) in the naphthyl group. We have demonstrated in this work how the careful control of the intermolecular aggregation process can modulate the competition between phosphorescence emission and energy transfer from the triplet state of the gold(I) complexes to produce singlet oxygen.

Introduction

Population of the triplet state in chromophores is an important aspect that plays a key role in numerous applications such as photodynamic therapy,[1] bioimaging,[2,3] photocatalysis,[4] light-emitting diodes (OLEDs)[5,6] and oxygen sensing[7,8] among others. In particular, singlet oxygen production stays at the forefront of research due to its reactivity as a synthetic reagent, as an intermediate in oxygenation reactions of polymers[9] or as a reactive oxygen species (ROS) for biological purposes.[10]

Singlet oxygen can be formed, for example, through sensitization, wherein a photosensitizer (PS) in the excited triplet state relaxes to its ground state by triplet energy transfer to ambient oxygen.[11] For this reason, photosensitizers that have a populated triplet excited state higher in energy but close to the lower excited state of oxygen, $^1O_2$, are of great interest to be explored in this field. Nevertheless, for efficient production, the sensitizers should possess additional features such as high intersystem crossing (ISC) rates and long triplet lifetimes in order to increase the probability of energy transfer. In terms of molecular design, ISC may be favoured by enhancing the spin–orbit coupling (SOC) with the introduction of heavy atoms[12–14] or heteroatoms[15,16] or by introducing donor/acceptor units with electron transfer steps.[17,18] In this way, organometallic chromophores containing heavy metals deserve their investigation in this field since they possess high SOC values and the tuneability of their photophysical properties through ligand modification can be easily performed.[19] Among all the metals used in the literature for singlet oxygen production, gold(I) is scarcely explored and only a few examples have been reported in the literature in this field.[20–23]

Supramolecular chemistry offers several advantages within this field. The majority of the published results use cavitands (such as curcubiturils, cyclodextrins or calixarenes) to encapsulate the photosensitizer in order to disrupt the aggregation process (aggregation-induced photo-deactivation) and enhance their singlet oxygen generation. Nevertheless, other techniques also can be found, such as the introduction of the photosensitizer within a polymer matrix together with iodine-containing hydrocarbon to enhance the singlet oxygen generation by the effect of an external heavy atom[24] or the co-encapsulation of a donor and acceptor within a polymer matrix which highly enhances the singlet oxygen production.[25]

Regarding this, gold alkynyl compounds play an important role as building blocks for the construction of luminescent supramolecular materials, where the linearity driven by alkynyl-chromophore ligand can also induce the presence of Au···Au aurophilic interactions. These interactions are especially important in the resulting intra- and/or intermolecular aggregation and, together with solubility can be able to tune the luminescent properties at low solubility conditions through aggregation induced emission (AIE).[26–28] Regarding this, phosphanes are suitable ligands to modulate the solubility and supramolecular assemblies of gold(I) complexes.[29–31]

Taking all these facts into consideration, in this work six new phosphane-gold(I)-4-ethynylaniline complexes (neutral

[a]Departament de Química Inorgànica i Orgànica, Secció de Química Inorgànica, Universitat de Barcelona, Martí i Franquès 1-11, E-08028 Barcelona, Spain
[b]Institut de Nanociència i Nanotecnologia (IN^{2}UB). Universitat de Barcelona, 08028 Barcelona, Spain. E-mail: andrea.pinto@qi.ub.es, laura.rodriguez@qi.ub.es
[c]Department of Chemistry, Nanoscience Center, University of Jyvaskyla, P.O. Box 35, 40014 Jyvaskyla, Finland
[d]Department of Chemistry, Loughborough University, Loughborough, Leics LE11 3TU, UK

†Electronic supplementary information (ESI) available. CCDC 2165920. For ESI and crystallographic data in CIF or other electronic format see DOI: https://doi.org/10.1039/d2dt01154a

and cationic) have been synthesized. The compounds contain a three tris-naphthalene substituted tertiary phosphane where the chromophore is coordinated to the phosphorus atom through a secondary amine which contain different halogens groups (Cl and Br) in the naphthyl moiety. The study of their luminescent properties, their supramolecular assemblies and the singlet oxygen generation are analysed in detail. These phosphanes are mainly interesting since they present intrinsic luminescence (thanks to the naphthyl groups), together with NH connectors (in the CH_2-NH chain between the P atom and the naphthyl) that may affect the resulting supramolecular assemblies and luminescent properties.

Results and discussion

Synthesis and characterization

The complexes **1–3** were synthesized by the reaction of the previously synthesized polymer $[Au(4\text{-ethynylaniline})]_n$ [32] and the corresponding P{CH_2-1-N(H)naphthyl}$_3$ phosphanes (Fig. S1†) previously synthesized following the reported experimental procedure[33] (Scheme 1). Several recrystallizations were needed to obtain the compounds in pure form rendering the products in moderate (50–60%) isolated yields.

The synthesis of the ionic complexes **4–6** followed the addition in two different steps of one equivalent of the corresponding phosphane to an initial solution of [AuCl(tht)] (Scheme 2).[34,35] The desired products were obtained in good yields of around 70–80%.

The characterization of complexes **1–6** by ^{1}H and ^{31}P{^{1}H} NMR and IR spectroscopies together with HRESI-MS(+) spectrometry evidences the correct formation of the desired products and their purity. The ^{1}H NMR spectra display the expected pattern of the phosphane and the aniline in the case of complexes **1–3**, whilst the ^{31}P{^{1}H} NMR spectra display a single resonance in all cases which is *ca.* 60 ppm downfield shifted with respect to the free phosphanes. IR spectra display the typical ν(C≡C) vibration at *ca.* 2100 cm^{-1} in the case of complexes **1–3** and ν(N–H) vibrations in all cases which are *ca.* 60 cm^{-1} shifted to higher wavenumbers upon coordination to the metal atom in all cases. Mass spectrometry analysis is an unequivocal final evidence for the correct formation of the desired products by the identification of the monoprotonated species $[M + H]^+$ and the $[M + Na]^+$ or $[M + K]^+$ species in the case of complexes **1–3** and the molecular peak $[M]^+$ in the case of **4–6** (see ESI†).

X-ray crystal structure determination

Single crystals of complex **5** suitable for X-ray diffraction were grown from methanol/diethyl ether. The compound crystallizes in the *C*2/*c* space group of the monoclinic crystal system. Selected bond lengths and angles are summarized in Table 1 and details of data collection and refinement in Table S1.†

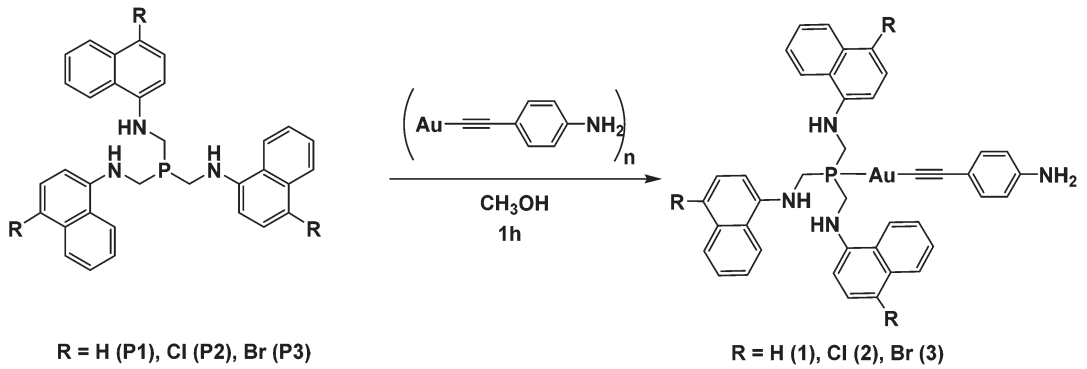

Scheme 1 Synthesis of the gold(I) complexes **1–3**.

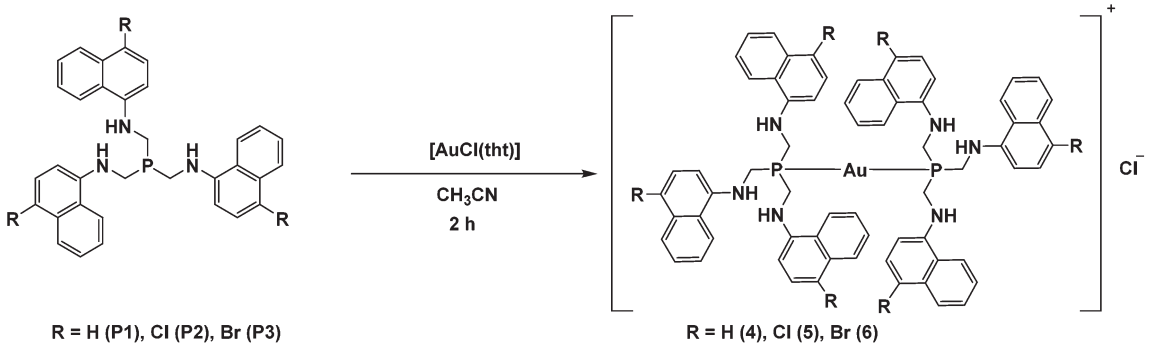

Scheme 2 Synthesis of gold(I) complexes **4–6**.

The asymmetric unit cell of complex **5** includes a half a molecule of **5** with two molecules of methanol (Fig. 1). A linear geometry is observed around the metal atom with a symmetry-enforced P–Au–P angle of 180° similar to other $[(PR_3)_2Au]Cl$ complexes.[36] The P–Au bond distance is in a good agreement with those found in other gold-phosphane complexes.[34,35] The P-CH_2-N angle is around 111° which is similar to other gold(I) complex with similar phosphanes[33] and is smaller with respect to the uncoordinated phosphane due to a higher steric hindrance when the gold(I) is coordinated and the phosphanes are in closer proximity to each other. The complex displays intramolecular short contacts N–H···Cl, Cl···π, Cl···Cl[37] in the 3D crystal packing. The packing arrangement shows that molecules form a chain due to the presence of hydrogen bonding of the N–H of the molecule, the chloride that acts as a counterion and the molecules of methanol present in the crystal structure (Fig. 2 and S20†). No Au···Au intermolecular contacts of note were observed between molecules of **5**.

Table 1 Selected bond lengths (Å) and angles (°) for **5**

Compound	Distance (Å)	Angle (°)
5	Au–P: 2.288(1) Au···Au: 12.193(1)	P–Au–P: 180.0(0) P–C–N: 111.1(3)

Photophysical characterization

The absorption and emission spectra of the uncoordinated phosphanes **P1–3** and the gold complexes **1–6** were recorded in 10^{-5} M dimethyl sulfoxide solutions at room temperature and the obtained data are summarized in Table 2.

The absorption spectra of all compounds (Fig. 3) display an absorption band at 320–350 nm that presents the same profile

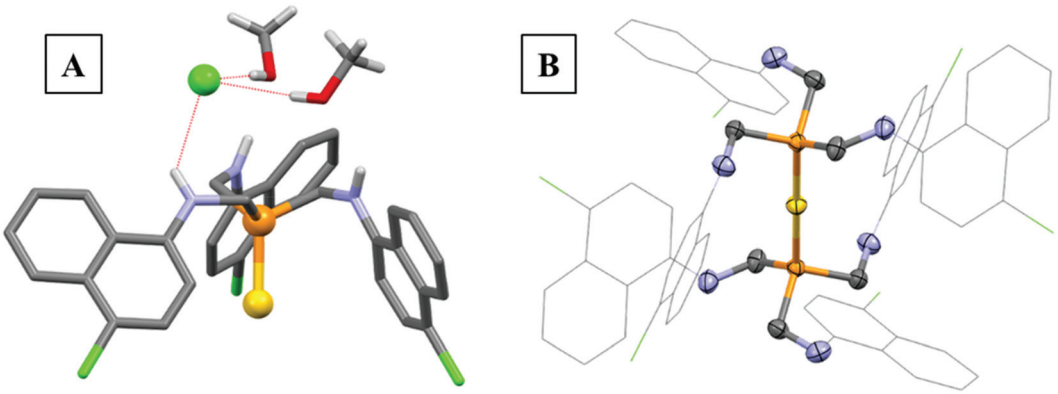

Fig. 1 X-Ray crystal structure of **5**. (A) Asymmetric cell showing hydrogen bonds; (B) complete cation with simplified naphthyl groups. Yellow: gold; orange: phosphorous; black: carbon; light blue: nitrogen; green: chlorine; red: oxygen (all C–H hydrogen atoms have been omitted for clarity).

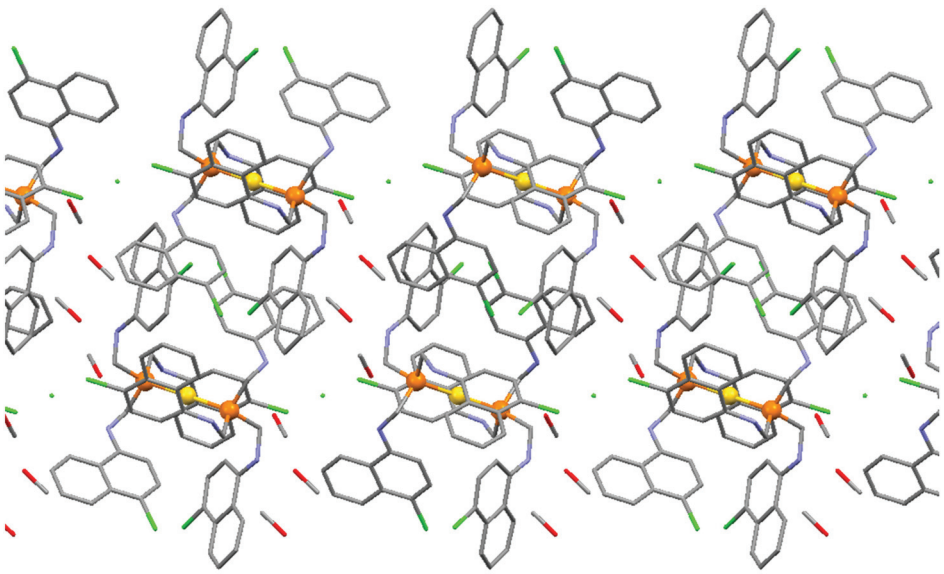

Fig. 2 Representation of the packing of **5**.

Table 2 Electronic absorption and emission data, quantum yield of complexes **1–6** and uncoordinated phosphanes in dimethyl sulfoxide

Compound	Absorption maxima λ_{max} (10^3 ε cm^{-1} M^{-1})	Emission maxima	Φ_F	τ_F (ns)	k_r (ns^{-1})	k_{nr} (ns^{-1})
P1	344 (23.5)	430	0.32	3.97	0.08	0.171
P2	360 (24.2)	446	0.26	2.82	0.092	0.262
P3	360 (21.6)	446	0.13	1.47	0.088	0.591
1	324 (34.4)	420	0.026	0.22	0.120	4.530
2	342 (27.3)	431	0.019	0.19	0.101	5.218
3	342 (28.3)	428	0.015	0.18	0.083	5.472
4	339 (25.9)	426	0.027	0.39	0.068	2.482
5	354 (26.5)	439	0.021	0.88	0.023	1.109
6	354 (41.2)	437	0.010	1.01	0.01	0.980

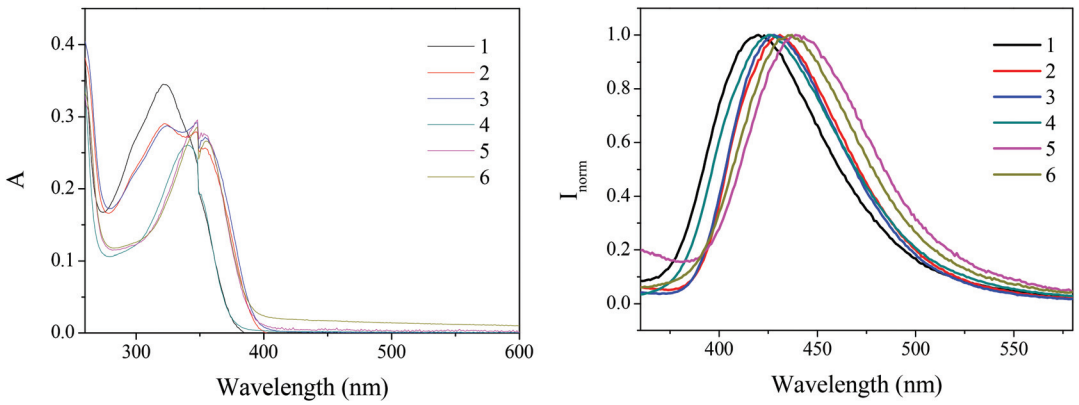

Fig. 3 Absorption (left) and normalized emission (right) spectra of complexes **1–6** in 1×10^{-5} M dimethyl sulfoxide solutions.

as the corresponding spectra of the **P1–3** phosphanes (Fig. S21†), but *ca.* 20 nm blue-shifted for the neutral complexes and about 5 nm for the ionic ones. Thus, this band can be assigned to the π–π* transition of the naphthyl chromophore of the phosphane. A similar trend is observed in the emission spectra upon excitation of the samples at the absorption bands. The recorded blue shift may be ascribed to the change on the closed conformation of the free phosphane (due to intramolecular N–H···N interactions) upon coordination to the metal atom that seems to be less affected in the bis(phosphane) derivatives due to steric hindrances. The broadening shape of the emission bands must be ascribed to interaction with solvents. Charge transfer processes are discarded since similar spectra recorded in dichloromethane display a vibronically structured shape with no shift of the emission maxima (see Fig. S23†).

A red shift is observed in all cases when a halogen is incorporated into the chemical structure of the naphthyl substituents (compounds **2**, **3**, **5** and **6**) in comparison with the unsubstituted analogous **1** and **4** due to an electronegativity effect. Such electronegativity effect occurs if either the HOMO or the LUMO is particularly stabilized, and it is especially pronounced in molecules with disjointed orbital structures, where the HOMO and LUMO are localized on different parts of the molecule.[38] Moreover, the effect of chlorine and bromine substituents on the resulting emission is almost identical. This is however consistent with the similar inductive and mesomeric properties of these two halogens (Br: $F = +0.45$, $R = -0.22$, Cl: $F = +0.42$, $R = -0.19$, F = field effect parameter, R = resonance parameter). That is, both substituents function as moderately inductive (σ) electron withdrawing group and as weak π-donor, as indicated by the Swain–Lupton parameters quantifying these two effects.[38,39]

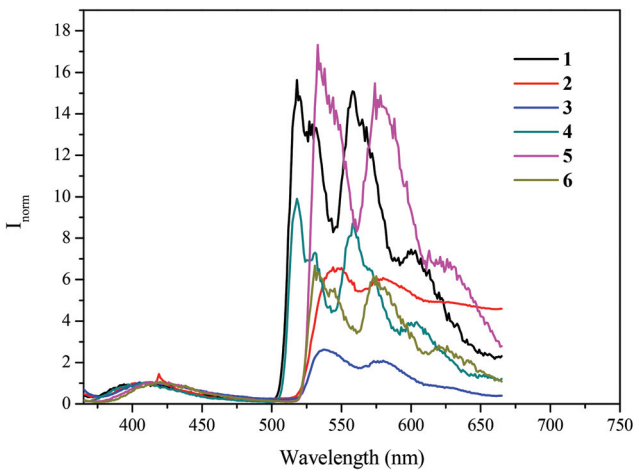

Fig. 4 Emission spectra of gold(I) complexes **1–6** at 77 K normalized at their fluorescence band.

Emission spectra recorded at 77 K in dimethyl sulfoxide (Fig. 4) show that only gold(I) complexes present phosphorescence at *ca.* 575 nm which is dominating the radiative process displaying only residual fluorescence emission (Fig. 4 and S24†). This is in agreement with the effect of the gold(I) as heavy atom to enhance the intersystem crossing and population of the triplet state. Curiously, the gold(I) compounds that contain **P3**, $P\{CH_2\text{-}1\text{-}NHC_{10}H_6(4\text{-}\mathbf{Br})\}_3$, (compounds **3** and **6**) display the lowest phosphorescent emission. This could be rationalized to the presence of this second heavy atom (bromine) that is also favouring faster non-radiative T1 → S0 deactivation. Additionally, we have observed that phosphorescence emission depends on concentration. As previously reported by Gray and co-authors,[40,41] this can be ascribed to the first population of a naphthalene excimer that lies higher on energy to the T1 state, to which it decays giving rise to the observed vibronically structured phosphorescence emission (see Fig. S25†).

The fluorescence quantum yields of the gold(I) complexes in dimethyl sulfoxide are between 1 and 3% and are one order of magnitude lower than those recorded for their phosphane precursors. The recorded values follow the trend R = H > Cl > Br, which is in agreement with the effect of the heavy halogen atom favouring the non-radiative deactivation processes. The lower fluorescence quantum yields observed for gold(I) compounds also confirms that gold(I) is populating the triplet state, which is much more favoured when a second heavy atom (Cl, Br) is included in the chemical structure of the molecule (Cl, Br). The radiative and non-radiative rate constants were calculated from the fluorescence quantum yields and lifetimes. In general, k_{nr} values are around 50-fold the corresponding k_r in the gold complexes while they are only 2 to 5-fold in the case of the free phosphanes, which is also in agreement with the recorded emission quantum yields.

Phosphorescence quantum yields, lifetimes and radiative and non-radiative rate constants were also calculated for gold(I) complexes at low temperature (77 K, Table S2†). The obtained values are quite high being larger for ionic compounds that can achieve near 60% emission efficiency and very long emission lifetimes of a few milliseconds. Gold(I) derivatives containing **P3** display the lowest phosphorescence quantum yield and lifetimes in agreement with the previous data. The calculated values of radiative rate constants for neutral gold(I) complexes (**1–3**) follow the trend R = H > Cl > Br while the non-radiative follows the inverse trend. On the contrary, the cationic compounds (**4–6**) barely differ on the calculated radiative and non-radiative rate constant between R = H and Cl.

Aggregation studies

It is well-known that gold(I) complexes tend to aggregate and that this process can be favored in solutions containing one good and one poorly miscible solvent in the former, such as water and DMSO.[28] Absorption and emission spectra were then measured in DMSO and in DMSO/water mixtures in order to find any possible evidences of aggregation and how it could affect their resulting luminescence.

A decrease and broadening of the absorption bands is observed for all compounds when the water contents increases, as a result from aggregation. The emission spectra is quenched at 90% water and it is *ca*. 30 nm red-shifted in the presence of water (see Fig. 5 and Fig. S26–32†). Emission spectra recorded at 77 K in DMSO/water (10/90) mixtures shows pure phosphorescence emission in the case of gold(I) complexes while only naphthalene fluorescence is recorded for the free phosphanes (see Fig. S33†). The complete disappearance of the fluorescence emission, which was residual in pure dimethyl sulfoxide solutions, indicates that the aggregation is promoting the intersystem crossing and enhances the triplet excited state population. This can be attributed to an increase of the structural rigidity on the molecule that limits the non-radiative pathways. The presence and size of the aggregates was analysed by dynamic light scattering (DLS) for all compounds in different water fractions (0%, 50% and 90%). The aggregates can be only detected from 50% water contents. As expected the size of the aggregates obtained from the phosphanes' solution is smaller (*ca*. 200 nm) than those detected for the gold(I) complexes. Additionally, in general, sizes are larger at 50% water contents than at 90% where the compounds are much more insoluble and can only form small insoluble aggregates that cannot be observed to the naked eye (Fig. S34–S42†).

In an attempt to obtain room temperature phosphorescence emission and reducing the non-radiative pathways, the gold(I) complexes **1–6** were introduced into SDS micelles and alginate matrixes (Fig. S43, S44 and Table S3†). Nevertheless, only fluorescence emission was recorded under these conditions as in solution. Interestingly, it can be observed that the emission of the encapsulated gold(I) complexes is more affected (red-shifted) than the spectra recorded for the free phosphanes which could be directly related to the intermolecular packing under these confined conditions.

Singlet oxygen production

The high phosphorescence emission recorded for the gold(I) complexes detected at low temperature together with the recorded decrease on the fluorescence quantum yields of gold (I) complexes and shorter decay times of their singlet excited states are clear evidences of the population of the triplet state being promoted by the Au(I) heavy atom effect. This fact encouraged us to analyze the potential of the compounds as singlet oxygen generators.

To confirm that gold(I) complexes can populate T_1 states *via* ISC also at room temperature, a reasonable approach is to use molecular oxygen as a triplet acceptor, which in turns generates oxygen *via* triplet–triplet state energy transfer. The generation of singlet oxygen can be done by the direct measurement of its well-known phosphorescence at 1270 nm. 1*H*-Phenal-1-one was used as standard reference in order to quantify this process (see Fig. S45†). The singlet oxygen quantum yield production values, Φ_Δ, (9–26%) (Table 3) obtained are moderate compared with other gold(I) complexes found in the literature.[20–23] Interestingly, the neutral gold(I) complexes that

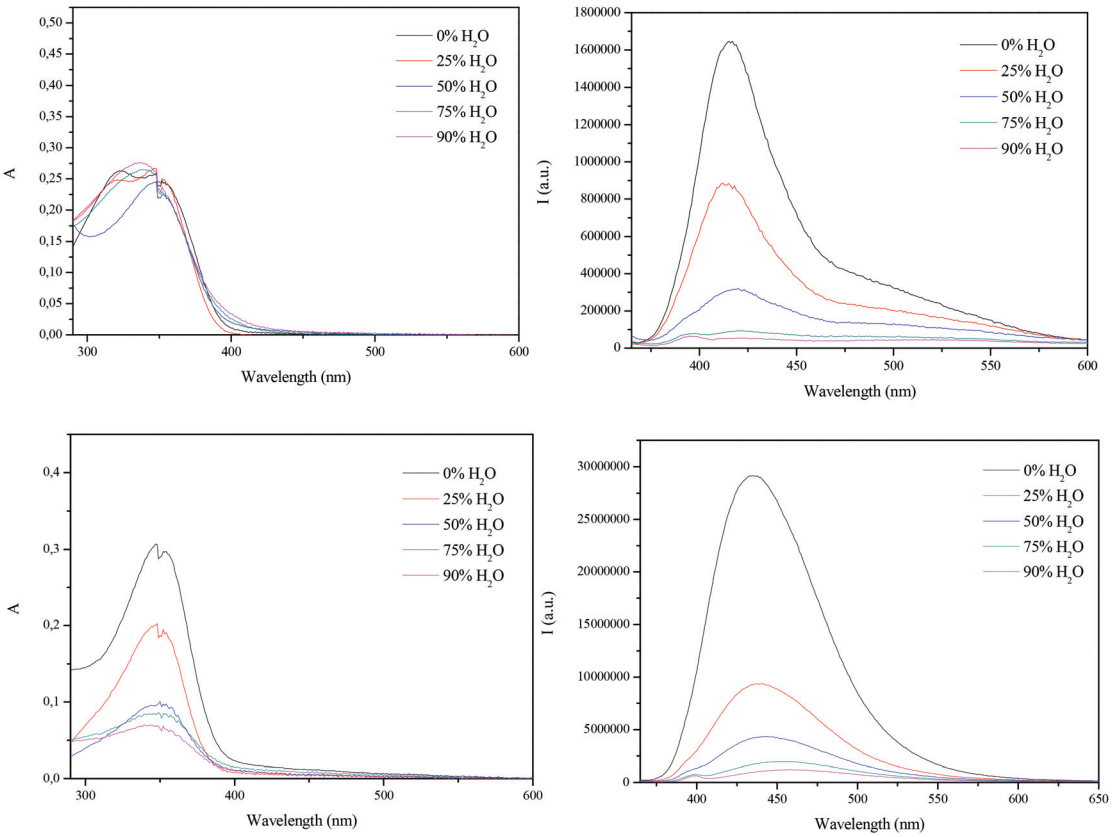

Fig. 5 Absorption (left) and emission (right) spectra of complex **2** (top) and **5** (down) in DMSO : water mixtures.

Table 3 Singlet oxygen sensitization quantum yield, Φ_Δ obtained in air-equilibrated in dichloromethane solutions for compounds **1–6**

Compound	Φ_Δ
1	0.21
2	0.26
3	0.17
4	0.11
5	0.09
6	0.09

contains 4-ethynilaniline as a ligand (**1–3**) display higher values of singlet oxygen sensitization. This can be correlated with the more efficient phosphorescence emission and aggregation process. As stated above, aggregation promotes the radiative deactivation pathway between the first triplet excited state and the ground state of the gold(I) complexes. This can be due to a competition between phosphorescence emission and energy transfer from the triplet state of molecules.[42] Therefore, the neutral gold(I) complexes **1–3** may aggregate less than the cationic compounds **4–6**. This is in agreement with the absorption spectra at different water contents, where the absorption band of the gold(I) complexes **4–6** decreases in a larger trend (see Fig. 5 and Fig. S26–32†).

The compounds that present the higher singlet oxygen production were also studied in alginate matrixes (see Fig. S46†). $^1O_2$ could not be detected neither in pure DMSO nor in water : DMSO mixtures, meaning that the structure of the matrix allows the disruption of the aggregation and therefore the $^1O_2$ detection. The recorded values are much lower than in dichloromethane, as expected for the lower solubility of oxygen in water, but interestingly, we have been able to find the adequate ways to produce $^1O_2$ in different media (polar and apolar) that could be relevant for specific desired applications (from reactivity or catalysis to more biological or green chemistry).

Conclusions

The study of the photophysical properties together with the aggregation process of six new phosphane-gold(I)-4-ethynylaniline complexes (neutral and cationic) revealed the efficient population of the triplet state of gold(I) derivatives being able to produce highly efficient phosphorescence which is not observed for the uncoordinated phosphanes. Additionally, the population of the triplet state has been also demonstrated since these gold(I) complexes can generate singlet oxygen in moderate to high yields. The introduction of the gold(I) complexes within gel matrixes has been of great relevance to also allow the production of singlet oxygen in more polar media

while it is not possible to detect in pure DMSO or water : DMSO mixtures.

Experimental section

General procedures

All manipulations were performed under prepurified N_2 using standard Schlenk techniques. All solvents were distilled from appropriate drying agents. 4-Ethynylamine (Aldrich, 97%), perinaphthenone (Aldrich, 97%) and alginic acid sodium salt (Aldrich) was used as received. Literature methods were used to prepare [AuCl(tht)],[43] P{CH_2-1-$NHC_{10}H_6$(4-H)}$_3$ (**P1**), P{CH_2-1-$NHC_{10}H_6$(4-Cl)}$_3$ (**P2**) and P{CH_2-1-$NHC_{10}H_6$(4-Br)}$_3$ (**P3**)[33] and [Au(C≡C-$C_6H_4NH_2$)]$_n$.[32]

Physical measurements

Infrared spectra were recorded on a FT-IR 520 Nicolet Spectrophotometer. ^{1}H-NMR (δ(TMS) = 0.0 ppm), ^{31}P{^{1}H}-NMR (δ(85% H_3PO_4) = 0.0 ppm) spectra were obtained on a Varian Mercury 400 and Bruker 400 (Universitat de Barcelona). ElectroSpray-Mass spectra(+) were recorded on a Fisons VG Quatro spectrometer (Universitat de Barcelona). Absorption spectra were recorded on a Varian Cary 100 Bio UV-spectrophotometer and emission spectra on a Horiba-Jobin-Ybon SPEX Nanolog spectrofluorimeter (Universitat de Barcelona). Luminescent quantum yields were recorded using an Absolute PL quantum yield spectrometer from Hamamatsu Photonics upon excitation the samples at 300 nm. Dynamic Light Scattering (DLS) measurements were carried out in a Zetasizer NanoS Spectrometer (Universitat de Barcelona).

Singlet oxygen yields. Room-temperature singlet oxygen phosphorescence was detected at 1270 nm with a Horiba-Jobin-Ybon SPEX Nanolog spectrofluorimeter (Universitat de Barcelona) using the DSS-IGA020L detector. The use of a Schott RG 1000 filter was essential to eliminate from the infrared signal all the first harmonic contribution of sensitizer emission in the region below 850 nm. The singlet oxygen formation quantum yield was then determined by direct measurement of the phosphorescence at 1270 nm following irradiation of the aerated solution in dichloromethane of the samples. Perinaphthenone in dichloromethane was used as standard reference, applying eqn (1).

$$\Phi_\Delta = \Phi_\Delta^{\mathrm{ref}} \frac{\mathrm{emission}_{1270\,\mathrm{nm}}}{\mathrm{emission}^{\mathrm{ref}}_{1270\,\mathrm{nm}}} \quad (1)$$

with $\Phi_\Delta^{\mathrm{ref}}$ the singlet oxygen formation quantum yield of the reference compound.[44]

Crystal data

X-ray data for **5** was measured using a Bruker-Nonius Kappa CCD diffractometer with an APEX-II detector with graphite-monochromatized Mo-Kα (λ = 0.71073 Å) radiation. Data collection and reduction were performed using the program COLLECT[45] and HKL DENZO AND SCALEPACK,[46] respectively, and the intensities were corrected for absorption using SADABS.[47] The structures were solved with intrinsic phasing (ShelXT)[48] and refined by full-matrix least squares on F^2 using the OLEX2 software,[49] which utilizes the ShelXL-2015 module.[50] Anisotropic displacement parameters were assigned to non-H atoms and isotropic displacement parameters for all H atoms were constrained to multiples of the equivalent displacement parameters of their parent atoms with U_{iso}(H) = 1.2U_{eq} (aromatic) or U_{iso}(H) = 1.5U_{eq} (alkyl) of their respective parent atoms. The X-ray single crystal data and CCDC number are included in Table S1.†

Synthesis and characterization

Synthesis of [Au(4-ethynylaniline)(P1)] (1). Solid **P1** (39 mg, 0.078 mmol) was added to a stirred suspension of [Au(C≡C-$C_6H_4NH_2$)]$_n$ (25 mg, 0.079 mmol) in methanol (10 mL) under N_2 atmosphere at room temperature. After 1 h of stirring, the solution was concentrated to the half and diethyl ether was added in order to favour the precipitation. The resulting yellow solid was filtered and dried under vacuum. Yield 51% (32 mg).

^{31}P{^{1}H}-NMR (dmso-d_6, 400 MHz): δ = 26.1 ppm; ^{1}H-NMR (dmso-d_6, 400 MHz): δ = 4.30 (d, J = 6.12 Hz, 6H, CH_2), 5.09 (s, 2H, NH_2), 6.35 (d, J = 8.64, 2H, H_α), 6.62 (m, 3H, Naph), 6.77 (d, J = 8.56 Hz, 2H, H_β), 6.86 (d, J = 7.56 Hz, 3H, Naph), 7.15 (d, J = 8.08 Hz, 3H, Naph), 7.22 (t, J = 7.68 Hz, 3H, Naph), 7.45 (m, 3H, Naph), 7.78 (d, J = 7.2 Hz, 3H, Naph), 8.14 (d, J = 7 Hz, 3H, Naph); IR (FT): ν = 3451 (s), 3349 cm^{-1} (s, N–H), 2101 (w, C≡C); ESI (+) m/z: 813.239 ([M + H]$^+$, calc: 812.234), 835.224 ([M + Na]$^+$, calc: 835.224), 851.201 ([M + K]$^+$, calc: 851.198).

Synthesis of [Au(4-ethynylaniline)(P2)] (2). Complex **2** was synthesized following the same experimental procedure reported for **1** but by using **P2** instead of **P1**. A yellow solid was obtained in a yield of 60% (43 mg).

^{31}P{^{1}H}-NMR (dmso-d_6, 400 MHz): δ = 25.3 ppm; ^{1}H-NMR (dmso-d_6, 400 MHz): δ = 4.27 (d, J = 5.36 Hz, 6H, CH_2), 5.05 (s, 2H, NH_2), 6.32 (d, J = 8.2 Hz, 2H, H_α), 6.72 (d, J = 8.2 Hz, 2H, H_β), 6.78 (d, J = 8.2 Hz, 3H, Naph), 7.28 (d, J = 8.3 Hz, 3H, Naph), 7.54 (t, J = 7.36 Hz, 3H, Naph), 7.61 (t, J = 8.12 Hz, 3H, Naph), 8.03 (d, J = 8.3 Hz, 3H, Naph), 8.20 (d, J = 8.3 Hz, 3H, Naph); IR (FT): ν = 3449 (s), 3353 cm^{-1} (s, N–H), 2103 (w, C≡C); ESI (+) m/z: 915.122 ([M + H]$^+$, calc: 915.117), 937.107 ([M + Na]$^+$, calc: 937.107), 953.079 ([M + K]$^+$, calc: 953.081).

Synthesis of [Au(4-ethynylaniline)(P3)] (3). Complex **3** was synthesized following the same experimental procedure reported for **1** but by using **P3** instead of **P1**. A purple solid was obtained in a yield of 59% (41 mg).

^{31}P{^{1}H}-NMR (dmso-d_6, 400 MHz): δ = 25.4 ppm; ^{1}H-NMR (dmso-d_6, 400 MHz): δ = 3.92 (d, J = 6.2 Hz, 6H, CH_2), 4.71 (s, 2H, NH_2), 5.97 (d, J = 8.4 Hz, 2H, H_α), 6.39 (d, J = 8.3 Hz, 2H, H_β), 6.41 (d, J = 8.4 Hz, 3H, Naph), 7.11 (d, J = 8.3 Hz, 3H, Naph), 7.18 (t, J = 7 Hz, 3H, Naph), 7.26 (t, J = 8.3 Hz, 3H, Naph), 7.64 (d, J = 7.8 Hz, 3H, Naph), 7.83 (d, J = 8.6 Hz, 3H, Naph); IR (FT): ν = 3453 (s), 3348 cm^{-1} (s, N–H), 2099 (w, C≡C); ESI (+) m/z: 1046.965 ([M + H]$^+$, calc: 1046.966), 1068.960 ([M + Na]$^+$, calc: 1068.956), 1084.942 ([M + K]$^+$, calc: 1084.930).

Synthesis of [Au(P1)$_2$]Cl (4). Complex **4** was prepared following the procedure previously reported in the literature[34] in a yield of 78% (77 mg).

^{31}P{^{1}H}-NMR (dmso-d_6, 400 MHz): δ = 15.9 ppm; ^{1}H-NMR (dmso-d_6, 400 MHz): δ = 3.79 (d, J = 5.7 Hz, 12H, CH_2), 6.70 (m, 12H, Naph), 7.07 (d, J = 8.2 Hz, 6H, Naph), 7.44 (m, 12H, Naph), 7.77 (d, J = 7.12 Hz, 6H, Naph), 8.13 (d, J = 7.76 Hz, 6H, Naph); IR (FT): ν = 3400 cm^{-1} (s, N–H); ESI (+) m/z: 1195.401 ([M]$^+$, calc: 1195.402).

Synthesis of [Au(P2)$_2$]Cl (5). Complex **5** was synthesized following the same experimental procedure reported for **4** but using **P2** instead of **P1**. A solid was obtained in a yield of 64% (72 mg).

^{31}P{^{1}H}-NMR (dmso-d_6, 400 MHz): δ = 11.3 ppm; ^{1}H-NMR (dmso-d_6, 400 MHz): δ = 3.91 (d, J = 4 Hz, 12H, CH_2), 5.71 (d, J = 8.3 Hz, 6H, Naph), 6.34 (d, J = 7.7 Hz, 6H, Naph), 7.00 (m, 6H, Naph), 7.62 (m, 6H, Naph), 7.97 (d, J = 8.04 Hz, 6H, Naph), 8.25 (d, J = 8.4 Hz, 6H, Naph); IR (FT): ν = 3410 cm^{-1} (s, N–H); ESI (+) m/z: 1399.162 ([M]$^+$, calc: 1399.168).

Synthesis of [Au(P3)$_2$]Cl (6). Complex **6** was synthesized following the same experimental procedure reported for **4** but using **P3** instead of **P1**. A solid was obtained in a yield of 75% (101 mg).

^{31}P{^{1}H}-NMR (dmso-d_6, 400 MHz): δ = 8.8 ppm; ^{1}H-NMR (dmso-d_6, 400 MHz): δ = 3.95 (d, J = 5.5 Hz, 12H, CH_2), 5.58 (d, J = 8.16 Hz, 6H, Naph), 6.36 (d, J = 8.12 Hz, 6H, Naph), 7.08 (m, 6H, Naph), 7.60 (m, 6H, Naph), 7.90 (d, J = 7.92 Hz, 6H, Naph), 8.25 (d, J = 8.3 Hz, 6H, Naph); IR (FT): ν = 3413 cm^{-1} (s, N–H); ESI (+) m/z: 1662.857 ([M]$^+$, calc: 1662.865).

Preparation of hydrogel beads doped with gold(I) complexes 1–6

Sodium alginate powder was dissolved in deionized (1.5% w/v) together with the gold(I) complex (10^{-5} M). Hydrogel beads were produced by extrusion of the alginate and gold(I) solution through a syringe into the gelling bath containing 250 mL of 0.1 M $CaCl_2$ solution.

Conflicts of interest

There are no conflicts to declare.

Acknowledgements

The authors are grateful to Project PID2019-104121GB-I00 funded by Ministerio de Ciencia e Innovación of Spain MCIN/AEI /10.13039/501100011033.

Notes and references

1 H. A. Collins, M. Khurana, E. H. Moriyama, A. Mariampillai, E. Dahlstedt, M. Balaz, M. K. Kuimova, M. Drobizhev, V. X. D. Yang, D. Phillips, A. Rebane, B. C. Wilson and H. L. Anderson, *Nat. Photonics*, 2008, **2**, 420–424.
2 S. Zhang, M. Hosaka, T. Yoshihara, K. Negishi, Y. Iida, S. Tobita and T. Takeuchi, *Cancer Res.*, 2010, **70**, 4490–4498.
3 F. Xiao, H. Gao, Y. Lei, W. Dai, M. Liu, X. Zheng, Z. Cai, X. Huang, H. Wu and D. Ding, *Nat. Commun.*, 2022, **13**, 186–196.
4 E. R. Sauvé, D. M. Mayder, S. Kamal, M. S. Oderinde and Z. M. Hudson, *Chem. Sci.*, 2022, **13**, 2296–2302.
5 S. Reineke, F. Lindner, G. Schwartz, N. Seidler, K. Walzer, B. Lüssem and K. Leo, *Nature*, 2009, **459**, 234–238.
6 Y. Miao, B. Zhao, Z. Gao, H. Shi, P. Tao, Y. Wu, K. Wang, H. Wang, B. Xu and F. Zhu, *Org. Electron.*, 2017, **42**, 1–7.
7 Z. Yang, S. Zhao, X. Zhang, M. Liu, H. Liu and B. Yang, *Front. Chem.*, 2022, **9**, 810304–810314.
8 W. J. Guo, Y. Z. Chen, C. H. Tung and L. Z. Wu, *CCS Chem.*, 2022, **4**, 1007–1015.
9 E. L. Clennan and A. Pace, *Tetrahedron*, 2005, **61**, 6665–6691.
10 S. G. Awuah and Y. You, *RSC Adv.*, 2012, **2**, 11169–11183.
11 P. R. Ogilby, *Chem. Soc. Rev.*, 2010, **39**, 3181–3209.
12 H. S. Kim, J. Y. Lee, S. Shin, W. Jeong, S. H. Lee, S. Kim, J. Lee, M. C. Suh and S. Yoo, *Adv. Funct. Mater.*, 2021, **31**, 2104646–2104657.
13 A. Rodriguez-Serrano, V. Rai-Constapel, M. C. Daza, M. Doerr and C. M. Marian, *Phys. Chem. Chem. Phys.*, 2015, **17**, 11350–11358.
14 C. Tang, P. Hu, E. Ma, M. Huang and Q. Zheng, *Dyes Pigm.*, 2015, **117**, 7–15.
15 H. Zhang, Y. Guo, Z. Wu, Y. Wang, Y. Sun, X. Feng, H. Wang and G. Zhao, *J. Lumin.*, 2021, **232**, 117864–117871.
16 G. H. Kim, R. Lampande, J. B. Im, J. M. Lee, J. Y. Lee and J. H. Kwon, *Mater. Horiz.*, 2017, **4**, 619–624.
17 A. Blacha-Grzechnik, M. Krzywiecki, R. Motyka and M. Czichy, *J. Phys. Chem. C*, 2019, **123**, 25915–25924.
18 M. L. Agazzi, J. E. Durantini, N. S. Gsponer, A. M. Durantini, S. G. Bertolotti and E. N. Durantini, *ChemPhysChem*, 2019, **20**, 1110–1125.
19 L. Bischoff, C. Baudequin, C. Hoarau and E. P. Urriolabeitia, *Adv. Organomet. Chem.*, 2018, **69**, 73–134.
20 S. Goswami, R. W. Winkel and K. S. Schanze, *Inorg. Chem.*, 2015, **54**, 10007–10014.
21 M. Üçüncü, E. Karakuş, E. K. Demirci, M. Sayar, S. Dartar and M. Emrullahoğlu, *Org. Lett.*, 2017, **19**, 2522–2525.
22 J. F. Longevial, K. El Cheikh, D. Aggad, A. Lebrun, A. van der Lee, F. Tielens, S. Clément, A. Morère, M. Garcia, M. Gary-Bobo and S. Richeter, *Chem. – Eur. J.*, 2017, **23**, 14017–14026.
23 A. Pinto, C. Cunha, G. Aullón, J. C. Lima, L. Rodríguez and J. S. Seixas de Melo, *J. Phys. Chem. B*, 2021, **125**, 11751–11760.
24 K. Naim, S. T. Nair, P. Yadav, A. Shanavas and P. P. Neelakandan, *ChemPlusChem*, 2018, **83**, 418–422.

25 S. Swaminathan, C. Fowley, E. R. Thapaliya, B. McCaghan, S. Tang, A. Fraix, B. Captain, S. Sortino, J. F. Callan and F. M. Raymo, *Nanoscale*, 2015, **7**, 14071–14079.
26 M. Rosental, R. N. Coldman, A. J. Moro, I. Angurell, R. M. Gomila, A. Frontera, J. C. Lima and L. Rodríguez, *Molecules*, 2021, **26**, 2444–2458.
27 A. J. Moro, J. Avó, M. Malfois, F. Zaccaria, C. Fonseca Guerra, F. J. Caparrós, L. Rodríguez and J. C. Lima, *Dalton Trans.*, 2020, **49**, 171–178.
28 A. Pinto, N. Svahn, J. C. Lima and L. Rodríguez, *Dalton Trans.*, 2017, **46**, 11125–11139.
29 M. Pujades and L. Rodríguez, *Coord. Chem. Rev.*, 2020, **408**, 213179–2131200.
30 M. C. Blanco, J. Cámara, V. Fernández-Moreira, A. Laguna and M. C. Gimeno, *Eur. J. Inorg. Chem.*, 2018, 2762–2767.
31 M. B. Smith, S. H. Dale, S. J. Coles, T. Gelbrich, M. B. Hursthouse and M. E. Light, *CrystEngComm*, 2006, **8**, 140–149.
32 N. Svahn, A. J. Moro, C. Roma-Rodrigues, R. Puttreddy, K. Rissanen, P. V. Baptista, A. R. Fernandes, J. C. Lima and L. Rodríguez, *Chem. – Eur. J.*, 2018, **24**, 14654–14667.
33 C. L. Carpenter-Warren, M. Cunnington, M. R. J. Elsegood, A. Kenny, A. R. Hill, C. R. Miles and M. B. Smith, *Inorg. Chim. Acta*, 2017, **462**, 289–297.
34 Z. Assefa, J. M. Forward, T. A. Grant, R. J. Staples, B. E. Hanson, A. A. Mohamed and J. P. Fackler Jr., *Inorg. Chim. Acta*, 2003, **352**, 31–45.
35 N. Svahn, I. Sanz, K. Rissanen and L. Rodríguez, *J. Organomet. Chem.*, 2019, **897**, 170–177.
36 G. A. Bowmaker, C. L. Brown, R. D. Hart, P. C. Healy, C. E. F. Rickard and A. H. White, *J. Chem. Soc., Dalton Trans.*, 1999, 881–890.
37 T. T. T. Bui, S. Dahaoui, C. Lecomte, G. R. Desiraju and E. Espinosa, *Angew. Chem., Int. Ed.*, 2009, **48**, 3838–3841.
38 A. L. Appleton, S. M. Brombosz, S. Barlow, J. S. Sears, J. L. Bredas, S. R. Marder and U. H. F. Bunz, *Nat. Commun.*, 2010, **1**, 1–6.
39 C. Hansch, A. Leo and R. W. Taft, *Chem. Rev.*, 1991, **91**, 165–195.
40 D. V. Partyka, A. J. Esswein, M. Zeller, A. D. Hunter and T. G. Gray, *Organometallics*, 2007, **26**, 3279–3282.
41 D. V. Partyka, M. Zeller, A. D. Hunter and T. G. Gray, *Angew. Chem., Int. Ed.*, 2006, **45**, 8188–8191.
42 L. Zang, H. Wang, Z. Wang, S. Wang, M. Yu, Q. Kang, G. Zou and H. Zhao, *J. Lumin.*, 2022, **244**, 118723–118729.
43 R. Usón and A. Laguna, *Organomet. Synth.*, 1986, **3**, 322.
44 N. Epelde-Elezcano, V. Martínez-Martínez, E. Peña-Cabrera, C. F. A. Gómez-Durán, I. López Arbeloa and S. Lacombe, *RSC Adv.*, 2016, **6**, 41991–41998.
45 R. W. W. Hooft, *COLLECT 1998*, Nonius BV, Delft, The Netherlands.
46 Z. Otwinowski and W. Minor, in *Methods in Enzymology, Macromolecular Crystallography, Part A*, ed. C. W. Carter Jr and R. M. Sweet, Academic Press, New York, 1997, vol. 276, pp. 307–326.
47 G. M. Sheldrick, *SADABS Version 2008/2*, University of Göttingen, Germany, 1996.
48 G. M. Sheldrick, *Acta Crystallogr., Sect. A: Found. Adv.*, 2015, **71**, 3–8.
49 O. V. Dolomanov, L. J. Bourhis, R. J. Gildea, J. A. K. Howard and H. Puschmann, *J. Appl. Crystallogr.*, 2009, **42**, 339–341.
50 G. M. Sheldrick, *Acta Crystallogr., Sect. C: Struct. Chem.*, 2015, **71**, 3–8.